Trace analysis of nitrated polycyclic aromatic hydrocarbons based on two-color femtosecond laser ionization mass spectrometry

Wen, Lu
Faculty of Design, Kyushu University

Yoshinaga, Katsunori
Faculty of Design, Kyushu University

Imasaka, Totaro
Kyushu University

Imasaka, Tomoko
Faculty of Design, Kyushu University

出版情報：Talanta. 265, pp.124807-, 2023-12-01. Elsevier
バージョン：
権利関係：

Supplementary Material

Trace analysis of nitrated polycyclic aromatic hydrocarbons based on two-color femtosecond laser ionization mass spectrometry

Lu WEN,[♯] Katsunori YOSHINAGA,[♯] Totaro IMASAKA,[†,‡] Tomoko IMASAKA[♯*]

[♯]*Faculty of Design, Kyushu University, 4-9-1, Shiobaru, Minami-ku, Fukuoka 815-8540: 744 Motooka, Nishi-ku, Fukuoka 819-0395, Japan*
[†]*Kyushu University, 744 Motooka, Nishi-ku, Fukuoka 819-0395, Japan*
[‡]*Hikari Giken, Co., 2-10-30, Sakurazaka, Chuou-ku, Fukuoka 810-0024, Japan*

Table of Contents

Experimental Procedures

Optimal temperature for a sample injection port of GC

It is known that nitro-PAHs partially decompose at a sample injection port of GC at high temperatures, and it is prefererable to set the temperature low to avoid this undesirable effect. On the other hand, the temperaure needs to be increased sufficiently to allow large nitro-PAHs with low volatilities to vaporize. The dependence of the signal intensity of the formation of a molecular ion on the temperature of the GC inlet port was examined to optimize the experimental conditions. As shown in Fig. S2, the temperature dependence was very different for each of the nitro-PAHs. The temperature of the GC injection port was therefore set at 280 ℃ in this sutdy as a compromise. It would be desirable to develop a technique to suppress the degradation of the nitro-PAHs in the sample injection port of GC in the future studies.

Computational approach

The spectral properties of nitro-PAHs were calculated based on density functional theory (DFT) with a cc-pVDZ basis set. Quantum chemical calculations were performed using a Gaussian16 program series package. Minimum geometries were obtained using the B3LYP method based on DFT with a cc-pVDZ basis set. The harmonic frequencies were calculated so as to ensure an optimum geometry providing a global energy minimum. A vertical ionization energy was evaluated from the difference between the energies of the ground and the ionic states, which were obtained at the level of ωB97XD/cc-pVTZ. The lowest one hundred singlet transition energies and the oscillator strengths were calculated using time-dependent DFT (TD-DFT) at the level of ωB97XD/cc-pVTZ, and the predicted absorption spectra were generated using the Gauss View 5 software program. The results are summarized in Fig. S3.

Two-photon detector based on mass spectrometry

The laser pulse width is an important parameter in the pump-and-probe experiment. The pulse width of the Yb laser (1030 nm) is reported to be 400 fs by the manufacturer. Autocorrelation and cross correlation techniques are currently used to evaluate the pulse width of the femtosecond laser, in which a nonlinear optical effect must be used for signal detection. Figure S5 shows the dependence of the signal intensity of the molecular ion of acetonitrile on the laser output power. The slope of the signal intensity against the laser power in a log-log plot was 1.8, suggesting NR2PI due to the absence of an absorption band at 343 and 257 nm. This result suggests that the present mass spectrometer can be used as a two-photon-response detector in an auto/cross correlator.

Pulse width measurment

Figure S6 shows the cross correlation trace obtained using the 343-nm and 257-nm pulses, in which the time delay was changed by translating the mechanical stage (see the Analytical instrument in the main text). Under the assumption of Gaussian pulses with same shapes for both the 343-nm and 257-nm pulses, the temporal pulse width (Δt) can be calculated from the full width at half maximum of the observed data ($\Delta \tau$) using the equation of $\Delta \tau / \Delta t = 1.41$, suggesting a laser pulse width being $\Delta t = 150$ fs in this study.

Figures

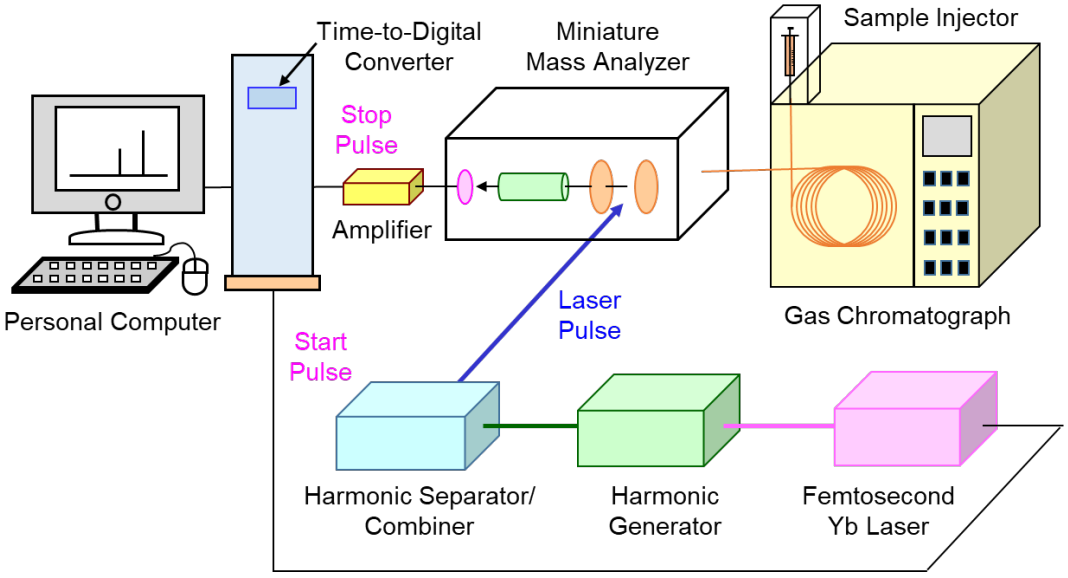

Figure S1. Block diagram of the experimental apparatus.

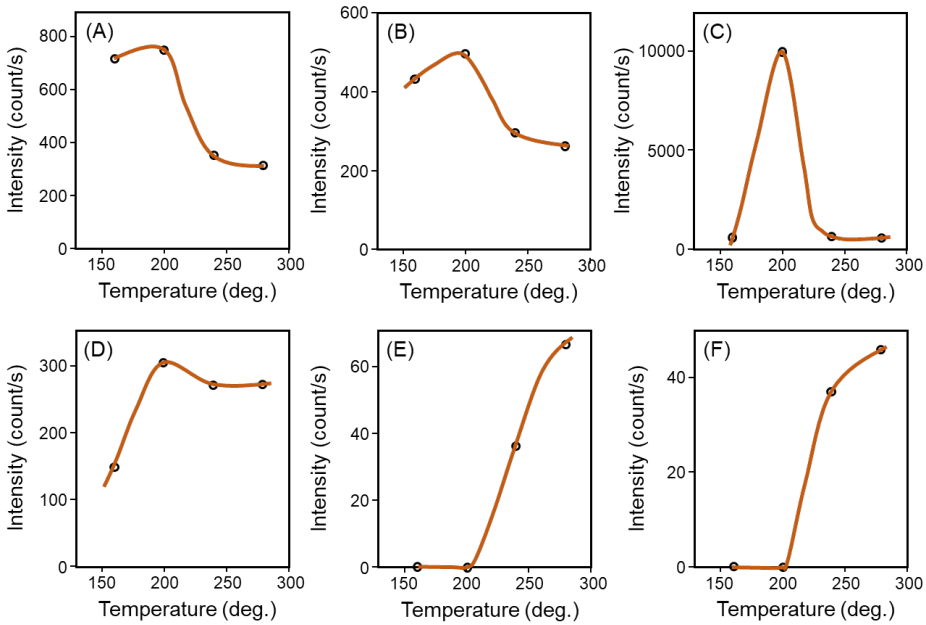

Figure S2. Dependence of the signal intensity of the molecular ion on the temperature of the sample injection port of GC. Sample; (A) 1-nitronaphthalene (B) 2-nitronaphthalene (C) 3-nitrobiphenyl (D) 2-nitrofluorene (E) 3-nitrofluoranthene (F) 1-nitropyrene. At low temperatures, larger nitro-PAHs with higher boiling points are more difficult to vaporize and to be introduced into the MS. On the other hand, smaller nitro-PAHs are more reactive at high temperatures and are decomposed in the sample injection port before introduction into the MS.

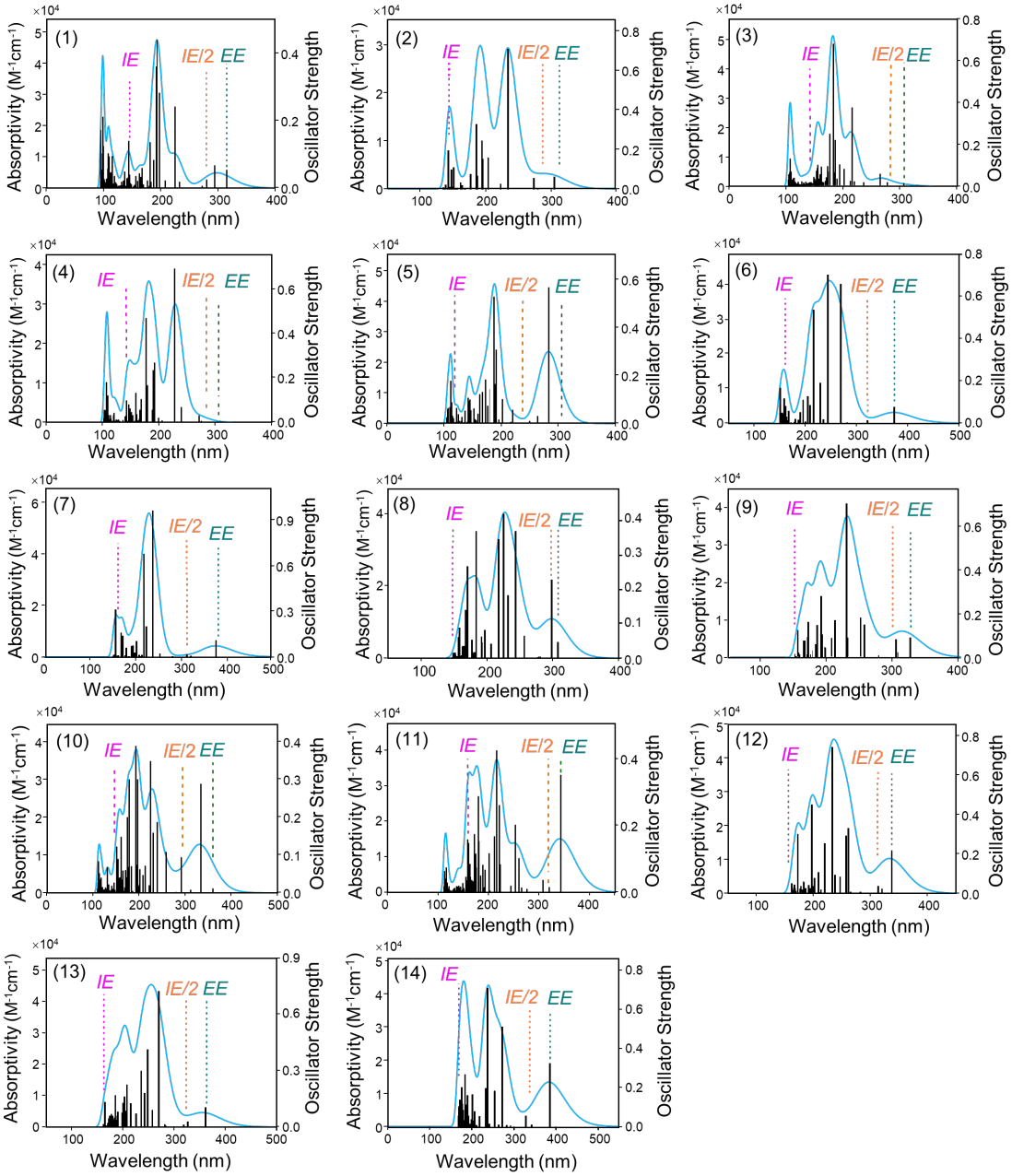

Figure S3. Absorption spectra of nitro-PAHs calculated by DFT. (1) 1-nitronaphthalene (2) 2-nitronaphthalene (3) 2-nitrobiphenyl (4) 3-nitrobiphenyl (5) 2-nitrofluorene (6) 2-nitroanthracene (7) 9-nitroanthracene (8) 3-nitrophenanthrene (9) 9-nitrophenanthrene (10) 3-nitrofluoranthene (11) 1-nitropyrene (12) 6-nitrochrysene (13) 7-nitrobenz(a)anthracene (14) 6-nitrobenzo(a)pyrene. *EE*, excitation energy, *IE*, ionization energy, *IE*/2, half value of *IE*.

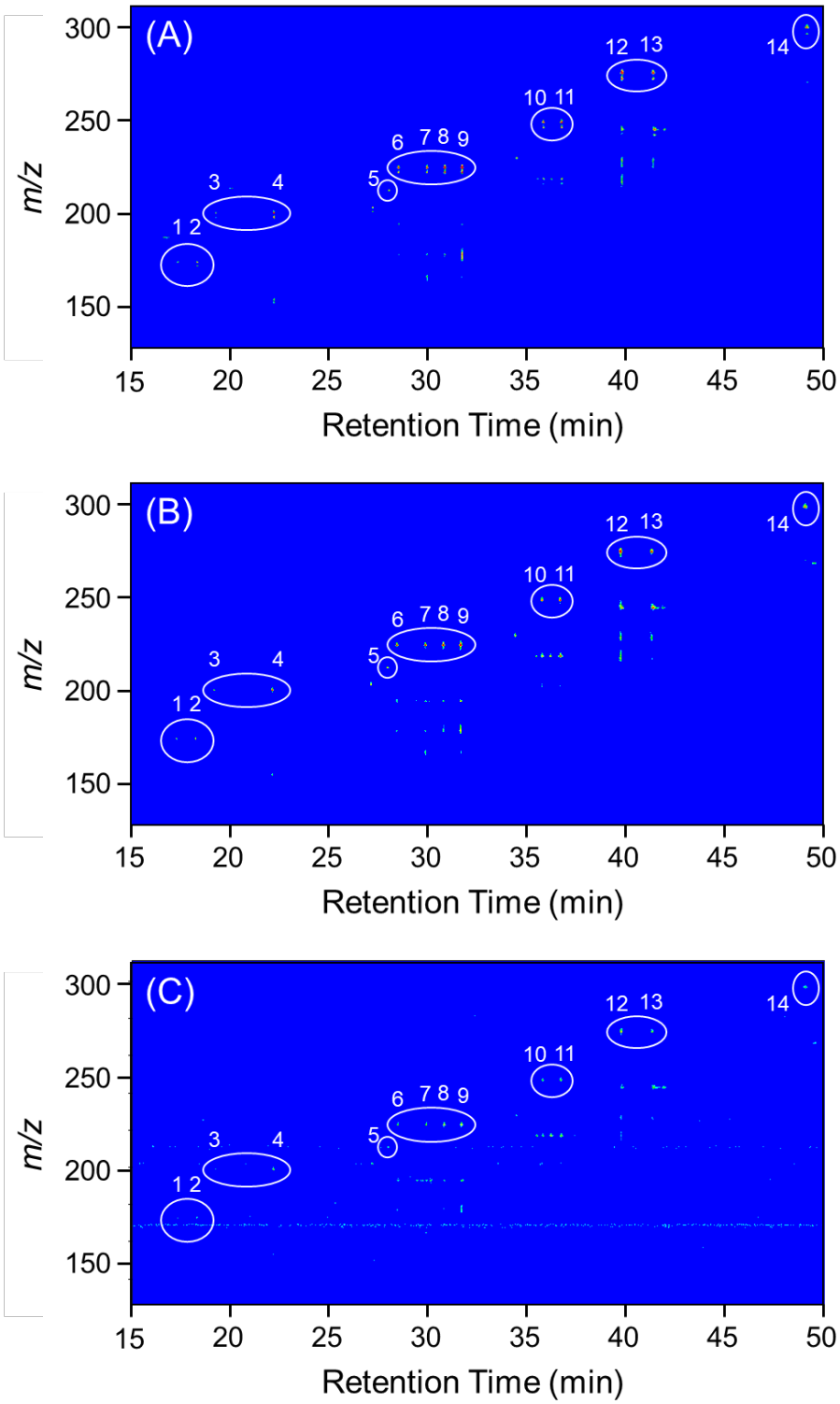

Figure S4. Two-dimensional display of GC-MS measured for a sample mixture containing 14 nitro-PAHs (6.5 ppm for each) at different wavelengths. (A) 343 nm (B) 257 nm (C) 206 nm. Laser output power; (A) 140 mW (B) 140 mW (C) 29 mW.

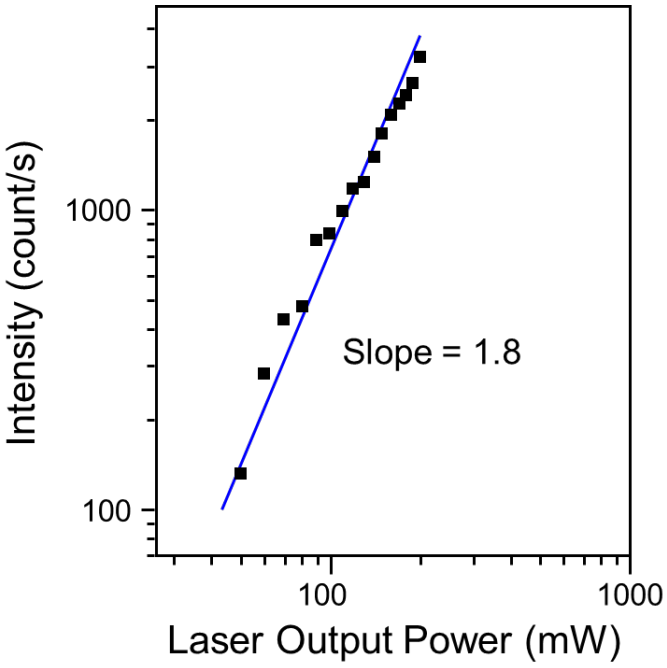

Figure S5. Dependence of the signal intensity of the molecular ion on the laser output power. The laser power was 90 mW at 343 nm and 110 mW at 257 nm at a total output power of 200 mW. The laser power was adjusted by changing the angle of the crystal for the second harmonic generation. A sample of acetonitrile was continuously introduced into the MS, which can be ionized through NR2PI under present conditions.

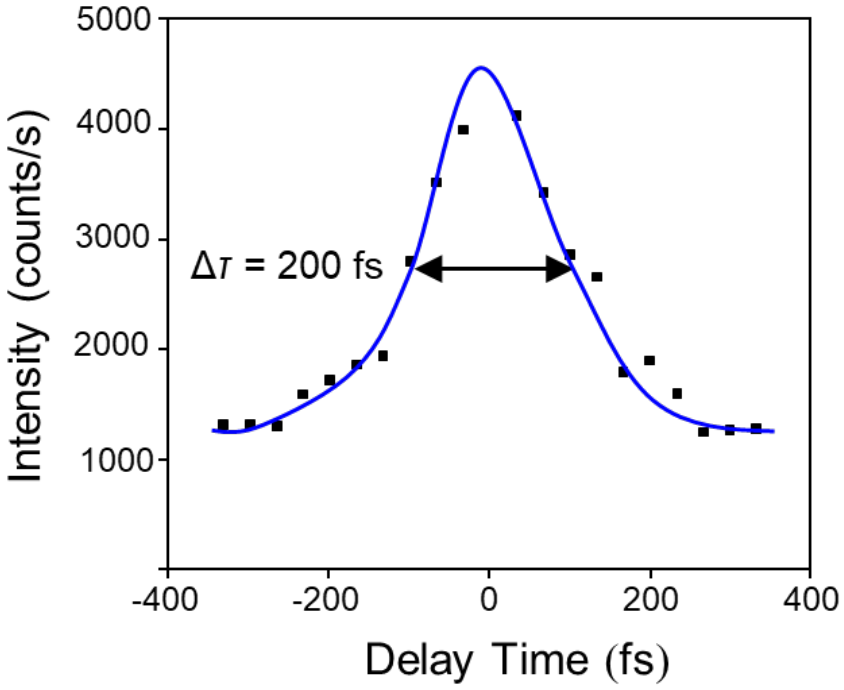

Figure S6. Cross correlation trace measured using two laser pulses emitting at 343 and 247 nm.

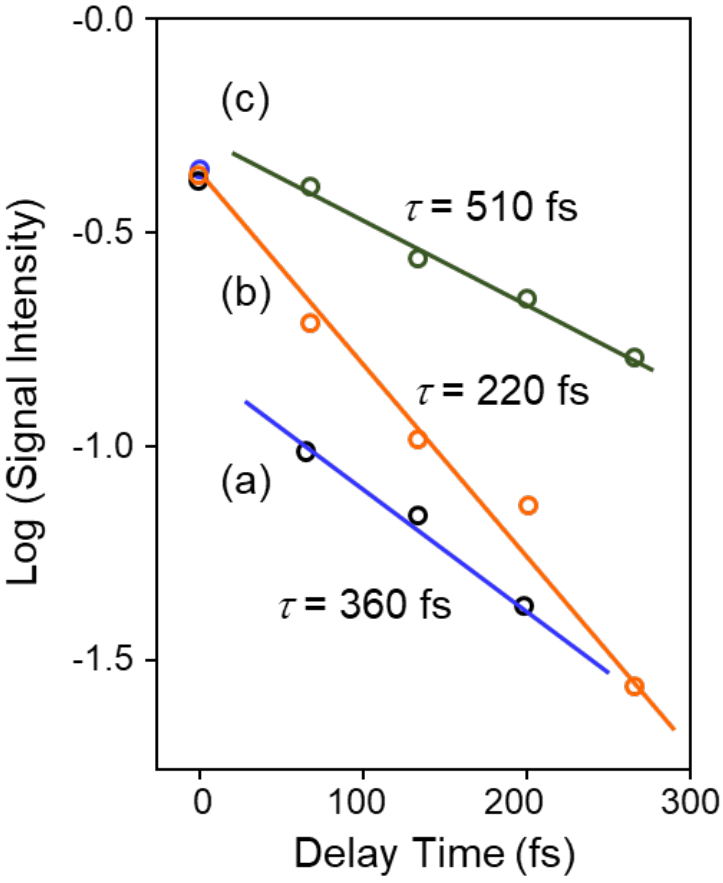

Figure S7. Dependence of the ratio of the signal intensities, $[M]^+/[F]^+$, on the delay time between the excitation and ionization pulses. The background signal arising from two independent pulses at 257 and 343 nm (see the broken line in Fig. 4) was subtracted from the observed data. The lifetimes calculated from decay curves (a) ~ (c) in Fig. 4 were evaluated from the slopes of the semi-log plots of the data and are shown in the figure.

Tables

Table S1

Spectral properties of 14 nitro-PAHs calculated by DFT

	Compound	Formula (Molecular Weight)	*IE* (eV)	*EE* (nm)	*EE* (eV)	Ionization Process				
						206 nm	257 nm	343nm	257 nm + 343 nm	343 nm + 257 nm
1	1-nitronaphthalene	$C_{10}H_7NO_2$ (173.2)	8.60	315	3.93	RE2PI	RE2PI	NR3PI	RE3PI	NR3PI
2	2-nitronaphthalene	$C_{10}H_7NO_2$ (173.2)	8.61	313	3.96	RE2PI	RE2PI	NR3PI	RE3PI	NR3PI
3	2-nitrobiphenyl	$C_{12}H_9NO_2$ (199.2)	8.74	307	4.04	RE2PI	RE2PI	NR3PI	RE3PI	NR3PI
4	3-nitrobiphenyl	$C_{12}H_9NO_2$ (199.2)	8.72	305	4.06	RE2PI	RE2PI	NR3PI	RE3PI	NR3PI
5	2-nitrofluorene	$C_{13}H_9NO_2$ (211.2)	10.45	306	4.06	RE2PI	RE3PI	NR3PI	RE3PI	NR3PI
6	2-nitroanthracene	$C_{14}H_9NO_2$ (223.2)	7.72	374	3.32	RE2PI	RE2PI	RE3PI	RE2PI	RE2PI
7	9-nitroanthracene	$C_{14}H_9NO_2$ (223.2)	7.72	378	3.28	RE2PI	RE2PI	RE3PI	RE2PI	RE2PI
8	3-nitrophenanthrene	$C_{14}H_9NO_2$ (223.2)	8.29	313	3.96	RE2PI	RE2PI	NR3PI	RE2PI	NR2PI
9	9-nitrophenanthrene	$C_{14}H_9NO_2$ (223.2)	8.35	324	3.82	RE2PI	RE2PI	NR3PI	RE2PI	NR2PI
10	3-nitrofluoranthene	$C_{16}H_9NO_2$ (247.3)	8.42	361	3.44	RE2PI	RE2PI	RE3PI	RE2PI	RE2PI
11	1-nitropyrene	$C_{16}H_9NO_2$ (247.3)	7.79	343	3.61	RE2PI	RE2PI	RE3PI	RE2PI	RE2PI
12	6-nitrochrysene	$C_{18}H_{11}NO_2$ (273.3)	7.94	338	3.67	RE2PI	RE2PI	NR3PI	RE2PI	NR2PI
13	7-nitrobenz(a) anthracene	$C_{18}H_{11}NO_2$ (273.3)	7.70	362	3.43	RE2PI	RE2PI	RE3PI	RE2PI	RE2PI
14	6-nitrobenzo(a)pyrene	$C_{20}H_{11}NO_2$ (297.3)	7.36	385	3.22	RE2PI	RE2PI	RE3PI	RE2PI	RE2PI

Two-photon energy; 6.02 eV (206 nm) × 2 = 12.04 eV, 4.81 eV (257 nm) × 2 = 9.63 eV, 3.61 eV (343 nm) × 2 = 7.22 eV, 4.81 eV (257 nm) + 3.61 eV (343 nm) = 8.43 eV. Three-photon energy; 4.81 eV (257 nm) + 3.61 eV (343 nm) × 2 = 12.04 eV, 3.61 eV (343 nm) × 3 = 10.83 eV. The value for *EE* calculated by DFT is usually larger than the observed value, and the NRMPI assigned at the boundary could then be categorized as REMPI (e.g., 3-nitrophenanthrene, 9-nitrophenanthrene, and 6-nitrochrysene).

Table S2
Concentration of nitro-PAHs determined for a sample extracted from diesel exhaust particulates (SRM1975).

	Compounds	Concentration NIST (mg/kg)[1)]	Concentration This study (mg/kg)[2)]
1	1-nitronaphthalene	0.013	1.22
2	2-nitronaphthalene	0.039	0.41
7	9-nitroanthracene	1.244	0.46
10	3-nitrofluoranthene	1.35	0.03
11	1-nitropyrene	16.59	0.63
12	6-nitrochrysene	0.85	0.07
13	7-nitrobenz(a)anthracene	1.68	2.32
14	6-nitrobenzo(a)pyrene	0.49	0.038

[1)] Non-certified values reported by NIST. [2)] A molecular ion was used for determination of nitro-PAHs in fs-LIMS.

Model and Equations

From Fig. 4 (A), the excitation and ionization processes can be expressed as follows.

$N_0 + h\nu_{(257)} \rightarrow N_1$

$N_1 + h\nu_{(343)} \rightarrow N_2$

where N_0, N_1, and N_2 show the ground, intermediate, and ionized states and $h\nu_{(257)}$ and $h\nu_{(343)}$ are the photons at 257 and 343 nm, respectively. The rate of production of the excited-state molecule can be calculated by equation (1), where $[N_1]$ is the population of the excited state, k_{1A} is the rate constant, $[N_0]$ is the population of the ground state, $I_{(257)}$ is the intensity of the laser pulse at 257 nm, k_{2A} is the rate constant for deactivation to the ground state, k_{3A} is the rate constant for ionization, and $I_{(343)}$ is the intensity of the laser pulse at 343 nm (see Fig. 4 (A)). The rate of production of the molecular ion can be calculated by equation (2), where $[N_2]$ is the population of the molecular ion.

$$\frac{d[N_1]}{dt} = k_{1A}[N_0]I_{(257)} - k_{2A}[N_1] - k_{3A}[N_1]I_{(343)} \quad (1)$$

$$\frac{d[N_2]}{dt} = k_{3A}[N_1]I_{(343)} \quad (2)$$

Equation (1) can be modified to equation (3).

$$\frac{d[N_1]}{dt} + K_1[N_1] = K_2 \quad (3)$$

where $K_1 = k_{2A} + k_{3A}I_{(343)}$ and $K_2 = k_{1A}[N_0]I_{(257)}$. In this study, K_2 is constant and time-independent, since the optical pulses at 257 (and 343 nm) can be assumed to be a delta function. Equations (3) can be solved to equation (4).

$$[N_1] = e^{-K_1 t}[\int e^{K_1 t}(K_2)dt + C] \quad (4)$$

$$= K_2 e^{-K_1 t}\left[\frac{e^{K_1 t}}{K_1} + \frac{C}{K_2}\right]$$

$$= \frac{K_2}{K_1}\left(1 + C\frac{K_1}{K_2}e^{-K_1 t}\right) \quad (5)$$

where C is the integration constant. When t = 0, equation (5) becomes equation (7).

$$[N_1]_0 = \frac{K_2}{K_1}\left(1 + C\frac{K_1}{K_2}\right) \quad \text{or} \quad C = [N_1]_0 - \frac{K_2}{K_1} \tag{6}$$

$$[N]_1 = [N_1]_0 e^{-K_1 t} + \frac{K_2}{K_1}(1 - e^{-K_1 t}) \tag{7}$$

where $[N_1]_0$ is the population of $[N_1]$ at immediately after excitation (t = 0). When the laser power was sufficiently small for both the pump and probe pulses, i.e., $I_{(257)} \cong 0$ and $I_{(343)} \cong 0$, $k_{2A} >> k_{3A} \times I_{(343)}$, the second term becomes nearly zero. Accordingly, equation (7) can be simplified to equation (8).

$$[N_1] = [N_1]_0 e^{(-k_{2A}t)} = [N_1]_0 e^{-\left(\frac{t}{\tau_A}\right)} \tag{8}$$

where τ_A (= $1/k_{2A}$) is the lifetime of excited state A. The intensity of the molecular ion can then be calculated using equation (9).

$$[N_2] = \int k_{3A}\,[N_1] I_{(343)} dt$$

$$[N_2] = k_{3A} I_{(343)} [N_1]_{t=DT}$$

$$= k_{3A} I_{(343)} [N_1]_0 e^{-(t_{DT}/\tau_A)} \tag{9}$$

where $[N_1]_{t=DT}$ is the population of excited state A at a delay time of t_{DT} from the pump pulse at 257 nm to the probe pulse at 343 nm. Then, the lifetime of excited state A, τ_A, can be evaluated by measuring the intensity of the molecular ion at different delay times. In a similar manner, the lifetime of excited state B, τ_B, can be evaluated by measuring the intensity of the molecular ion at different delay times from the pump pulse at 343 nm to the probe pulse at 257 nm using equation (10).

$$[N_2] = k_{3B} I_{(257)} [N_1]_0 e^{-(t_{DT}/\tau_B)} \tag{10}$$

The background signals arising from single-color two-photon/three-photon ionizations (not shown in Fig. 4 (A) and (B)) are superimposed on the signal arising from two-color two-photon ionization, which are independent of the delay time. The contribution of these

signals should be subtracted before data analysis. In addition, the signal intensity of the molecular ion varies with change in the ionization efficiency (e.g., by instabilities in the output power and the pulse width of the laser) and with a change in the concentration of the analyte in the ionization region (e.g., by instabilities in the laser beam pointing and amount of samples injected into GC), since the GC-MS measurement should be repeated ca. 10 times at different delay times and more than 10 hr was needed for a series of experiments to be performed. In order to (partially) cancel such the changes in the experimental conditions, the ratio of the signal intensities for the molecular ion, $[M]^+$, and the fragment ion, $[F]^+$, was calculated as follows.

$$\frac{[M]^+}{[F]^+} = \frac{[M]^+_{257/343} + [M]^+_{343/257} + [M]^+_{257/257} + [M]^+_{343/343}}{[F]^+_{257/343} + [F]^+_{343/257} + [F]^+_{257/257} + [F]^+_{343/343}} \quad (11)$$

In equation (11), the subscript of 257/343 (343/257) indicates that the pump pulse at 257 nm (343 nm) reaches the analyte earlier than the probe pulse at 343 nm (257 nm) in two-color ionization. On the other hand, the subscript of 257/257 (343/343) indicates single color ionization at 257 nm (343 nm). The term, $[M]^+_{257/343} + [M]^+_{343/257}$, is dependent of t_{DT}, and the term, $[M]^+_{257/257} + [M]^+_{343/343}$, are independent of t_{DT}. Similarly, the term, $[F]^+_{257/343} + [F]^+_{343/257}$, is dependent of t_{DT}, which is much smaller than the t_{DT}-independent term, $[F]^+_{257/257} + [F]^+_{343/343}$, since the excess energy is minimal for two-color two-photon ionization of 1-nitronaphthalene and 3-nitrofluoranthene examined in this study (see Table S1). Accordingly, equation (11) can be simplified to equation (12).

$$\frac{[M]^+}{[F]^+} = \frac{[M]^+_{257/343} + [M]^+_{343/257} + K_3}{K_4} \quad (12)$$

$$K_3 = [M]^+_{257/257} + [M]^+_{343/343}$$

$$K_4 = [F]^+_{257/343} + [F]^+_{343/257} + [F]^+_{257/257} + [F]^+_{343/343}$$

$$\cong [F]^+_{257/257} + [F]^+_{343/343}$$

Equation (12) can be modified to

$$\frac{[M]^+}{[F]^+} = \frac{[M]^+_{257/343} + K_3}{K_4} \quad (t_{DL} \leq 0) \quad (13)$$

$$\frac{[\mathrm{M}]^+}{[\mathrm{F}]^+} = \frac{[\mathrm{M}]^+_{343/257} + \mathrm{K}_3}{\mathrm{K}_4} \quad (t_{DL} \geq 0) \tag{14}$$

Equations (13) and (14) can be modified to equations (15) and (16) using equations (9) and (10), respectively, since $[N_2] = [\mathrm{M}]^+_{257/343}$ at $t_{DL} \leq 0$ and $[N_2] = [\mathrm{M}]^+_{343/257}$ at $t_{DL} \geq 0$.

$$\frac{[\mathrm{M}]^+}{[\mathrm{F}]^+} \propto e^{-(t_{\mathrm{DT}}/\tau_{\mathrm{A}})} + \mathrm{K}_5 \quad (t_{\mathrm{DT}} \leq 0) \tag{15}$$

$$\frac{[\mathrm{M}]^+}{[\mathrm{F}]^+} \propto e^{-(t_{\mathrm{DT}}/\tau_{\mathrm{B}})} + \mathrm{K}_5 \quad (t_{\mathrm{DT}} \geq 0) \tag{16}$$

where K_5 is a constant and independent of t_{DT}. In order to measure the excited state lifetime, the contribution of the term independent of the delay time should be subtracted from the data of $[\mathrm{M}]^+/[\mathrm{F}]^+$ and be plotted against the delay time of the probe pulse. The slope of the semi-log plot provides a decay rate, which is inversely proportional to the lifetime of the excited state (see Fig. S7).